




# Attempt to tune the dielectric and optical properties in PVA/ZnO composite using tetra ethylene glycol dimethyl ether for light emitting devices

O. Elkalashy<sup>1</sup> · E. Sheha<sup>2</sup> 

Received: 30 May 2018 / Accepted: 5 July 2018 / Published online: 19 July 2018  
© Springer-Verlag GmbH Germany, part of Springer Nature 2018

## Abstract

Tuning the dielectric constant of the optical materials is of prime importance to optimize their efficiency. Polyvinyl alcohol and tetra ethylene glycol dimethyl (TEGDME) matrix hybrid nanocomposites, featuring zinc oxide embedded in the polymer were fabricated by solution casting technique. TEM images showed that the introduction of tetra ethylene glycol dimethyl ether reduces the dimensions of ZnO particles and displays good distribution of the zinc oxide nanoparticles with very little particle agglomeration, respectively. The presence of tetra ethylene glycol dimethyl ether increases the optical energy gap of the composite from 3.6 to 4 eV. The Intensity and broadening of photoemission increase with increasing the ratio of TEGDME. The  $I$ - $V$  measurements of the fabricated Cu/(PVZO/TEGDME)/Cu cell under different sun light intensity revealed that the resistivity of the composite decreases with increasing sun light intensity and the presence of tetra ethylene glycol dimethyl ether reduces the resistivity and increases the sensitivity of the composite to sun light. The tunable dielectric constant and optical properties of these polymer composites are demonstrated by increasing the TEGDME contents in the composites, making these composites potentially useful for optimizing optical and electronic devices.

## 1 Introduction

Light emitting diode (LED) in its simplest form is a semiconductor p-n junction device (chip) that, when forward biased, emits photons (light) as the electrons and holes recombine near the junction [1, 2]. For some times, the uses of LED were limited on indicator lights and numeric displays on consumer electronic devices due to its low output and lack of its color options. Recently, the development of new LED materials and improved production processes have produced bright LEDs in colors throughout the visible spectrum, including white light [1]. LEDs are finding their way into many new applications such as advertisement, automobile lights, traffic lights and in general lighting applications [2, 3]. Light-emitting diodes (LEDs) based on wideband gap

semiconductor have attracted considerable attention due to their potential optoelectronic applications in illumination. Among the available wide band gap semiconductors is zinc oxide (ZnO), with a large direct band gap of 3.37eV [4–6]. It is nontoxic, chemically stable, and has low cost [7], high electron mobility, and strong room-temperature luminescence [8]. It has unique band structure and large exciton binding energy of about 60 meV [5, 9]. It also has desirable properties for light emission, particularly ZnO nanorods (NRs), due to the increased junction area, reduced temperature sensitivity, enhanced polarization dependence of reflectivity, and improved carrier confinement in one dimensional (1D) nanostructures [10]. These unique properties make this material a promising candidate for its applications in light-emitting diodes [7]. Recently, there has been a great deal of worldwide interest and research aiming to develop new technologies in the field of alternative energy and production of highly-efficient reliable LED crystals with increased capacity. So, researchers have since then been interested in improving the optical, electrical and dielectric properties of materials which are promising candidates in LED application.

Relative dielectric constant ( $\epsilon_r$ ) is one of the important factors which play a critical role in performance of LED

✉ E. Sheha  
islam.shihah@fsc.bu.edu.eg

<sup>1</sup> Photometry and Radiometry Division, Photometry Department, National Institute of standards (NIS), Giza 136, Egypt

<sup>2</sup> Physics Department, Faculty of Science, Benha University, Benha 13518, Egypt

[11]. Dielectric tunable polymer composites are highly desirable; the dielectric constant of medium significantly influences the exciton binding energy and the resulting charge separation and recombination, thereby boosting short-circuit current densities ( $J_{sc}$ ) and power conversion efficiencies (PCEs) [12]. Several different approaches have been tried to enhance the  $\epsilon_r$  value of organic semiconductors. The dielectric constant of organic/polymeric materials can be increased by incorporation of polar substituents such as nitrile, azide [12]. Aleshin et al. reported a solution-processed polyfluorene (PFO)–ZnO nanoparticles composite light-emitting organic field-effect transistor (LE-OFET). The ambipolar PFO:ZnO LEOFET emits light at both positive and negative gate bias [13]. The role of the annealing temperature at 80 °C on polymer solar cells (PSCs) was found to possess optimal blend morphology favorable for efficient charge separation owing to reduced coulomb capture radius and relatively high dielectric constant, resulting in high power conversion efficiency (PCE) of ~ 11.4 [14]. The addition of small molecules with a high  $\epsilon_r$ , camphoric anhydride into *B,O*-chelated azadipyrromethane (BO-ADPM) donor films, results in an increase in the  $\epsilon_r$  of BO-ADPM film from ~ 4.5 to ~ 11 [12]. Five fluorinated naphthalene diimide (NDI)-based acceptor polymers, with different content of fluorine were synthesized. The incorporation of fluorine increased the  $\epsilon_r$  of the acceptor polymers and blend films, which improved the charge generation and photocurrent [11]. Tetra ethylene glycol dimethyl ether (TEGDME) is a polar versatile solvent with excellent chemical and thermal stability [15, 16]. It has high boiling point and higher specific capacity as compared to carbonates and other ethers [17]. It displays a high  $\text{LiPF}_6$  solubility to produce well-conducting solutions with a wide electrochemical window [17]. TEGDME is also used in lithium-ion battery technology and is combined with trifluoroethanol as a working pair for organic absorption heat pumps [15, 16]. Generally, tuning dielectric constant is one of the major factors which plays a critical role in the performance of light emitting devices. The tunable dielectric properties and high robustness of polymer composites make them promising candidates for electronic devices with low power consumption. In the present paper, TEGDME has for the first time been originally introduced as a new modifier to optical composite. Our innovative aspect is based on using the aforesaid features of TEGDME to modulate the dielectric constant and optical properties of polyvinyl alcohol/zinc oxide composite. The composite films were prepared using easy and low cost solution casting method. The structure of the samples was characterized by X-ray diffraction, transmission electron microscopy and infrared spectroscopy. The physical and optical properties were characterized by UV–visible spectroscopy, photoluminescence

spectroscopy and thermal gravimetric analysis. The electrical properties of the samples were characterized using impedance spectroscopy.

## 2 Experimental

Poly vinyl alcohol (PVA) 98–99% hydrolyzed [QualiKems chemical company (India)], Zinc oxide (ZnO) (Alfa Aesar) and tetra ethylene glycol dimethyl ether (TEGDME) ( $\text{C}_{10}\text{H}_{22}\text{O}_5$ ) (Alfa Aesar) were used without further purification. PVA/ZnO composite was prepared in the form  $\text{PVA}_{(0.9975)}/\text{ZnO}_{(0.0025)}$  PVZO according to reference [2]. Different concentrations of the TEGDME were added to the solution of PVZO polymer composite and stirred for 3 h at 70 °C until complete homogeneity was achieved to get PVZO/*x*TEGDME where *x* = (0, 2, 3, 4 and 5) ml. The resulting slurry was casted in petri dishes and allowed the water to evaporate slowly at room temperature till the traces of the solvent completely disappeared. The crystalline nature of composite films were investigated by X-ray diffraction model (EMPYREAN, PANALYTICAL) equipped with  $\text{Cu K}_\alpha$  as radiation source ( $\lambda = 1.54 \text{ \AA}$ ). The diffractograms were obtained in the following conditions  $2\theta = (10^\circ\text{--}70^\circ)$ , 40 kV and 30 mA. The chemical modification of PVZO composite due to TEGDME doping was achieved using Nicolet 380 Fourier transformer infrared spectroscopy. Transmission electron microscopy (TEM) studies were carried out using JEM/2100 TEM. The thermogravimetric analysis (TGA) was investigated with SHIMADZU TGA-50 thermal analyzer, in the temperature range of 20–400 °C, under a nitrogen atmosphere and at a heating rate of 20°C/min. The optical properties of PVZO/*x*TEGDME colloidal in water were obtained using Shimadzu spectrophotometer (310 pc), range 190–1200 nm. The photoluminescence (PL) spectrum was obtained with spectrofluorometer model (Jasco FP-6500, JAPAN). The dielectric properties and AC conductivity were measured using GW INSTRON (LCR-8110G) LCR meter. The measurements were carried out in the frequency range (20 Hz–10 MHz). The *I*–*V* measurements of the samples were measured by KEITHLEY (4020 source meter). The measurement occurred under different sunlight intensity using solar simulator 250 W (domestic source).

## 3 Results and discussion

The X-ray diffraction pattern PVZO/*x*TEGDME polymer composite is shown in Fig. 1a. The X-ray diffraction pattern of PVZO composite exhibited a broad peak at approximately  $2\theta = 19.4^\circ$  [18] and a small peak at  $40.7^\circ$  which were due to the semi crystalline structure stemming from the strong hydrogen bond interaction between the hydroxyl groups of

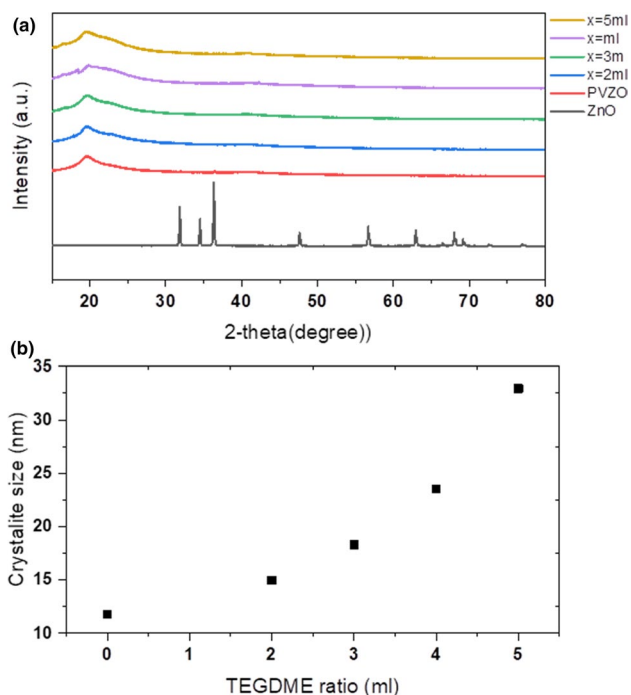


**Fig. 1** a X-ray diffraction pattern of PVZO/*x*TEGDME polymer composite. b The crystallite size of PVA polymer composite vs. TEGDME content

the PVA [7, 19]. In addition, small peaks were observed at  $2\theta = 31.79^\circ, 34.67^\circ$  and  $36.49^\circ$  corresponding to reflections from 100, 002 and 101 crystal planes, which confirmed the presence of the wurtzite ZnO crystal structure [JCPDS

Card No. 36-1451] [6, 19–21]. The ZnO peaks disappeared completely and PVA peaks became stronger and sharper after TEGDME modified the PVZO matrix as shown in Fig. 1a. TEGDME reacted with PVA forming low molecular weight co-polymer which had a high periodicity of hydroxyl groups and this behind the increase in the intensity of  $19.4^\circ$  peak. The values of the crystallite size of PVZO matrix were calculated using Scherer formula  $D = \frac{K\lambda}{\beta \cos \theta}$  [19, 22], where  $\lambda$  is the wavelength of the X-ray used ( $\lambda = 1.541 \text{ \AA}$ ),  $k \sim 0.9$  is the shape factor,  $\beta$  is the FWHM of the diffraction peak and  $\theta$  is the diffraction angle in degree. Figure 1b shows the impact of TEGDME on the crystallite size of PVA reflection plane. Gradual increase was observed in its values with increasing the ratio of TEGDME in PVZO matrix. This suggests that, TEGDME caused an increase in PVZO composite crystallinity as mentioned before. The calculated values of the crystallite size of ZnO were  $\sim 56 \text{ nm}$  for the pristine, and attended to very low values after modification by TEGDME. This affirms that TEGDME had the ability to dissolve ZnO particles to nano-scale causing the disappearance of ZnO peaks as confirmed by TEM results [18].

The FT-IR spectra of PVZO/*x*TEGDME polymer composite are shown in Fig. 2. The assignments and transference of FTIR peaks are summarized in Table 1. As shown, the O-H stretching vibration of PVZO composite [23] at  $3623 \text{ cm}^{-1}$  was transferred to high order of wavenumbers after modifying by TEGDME. The peak at  $1722 \text{ cm}^{-1}$  designated as a C=O stretching vibration [22] of PVZO composite was transferred to low order of wavenumbers

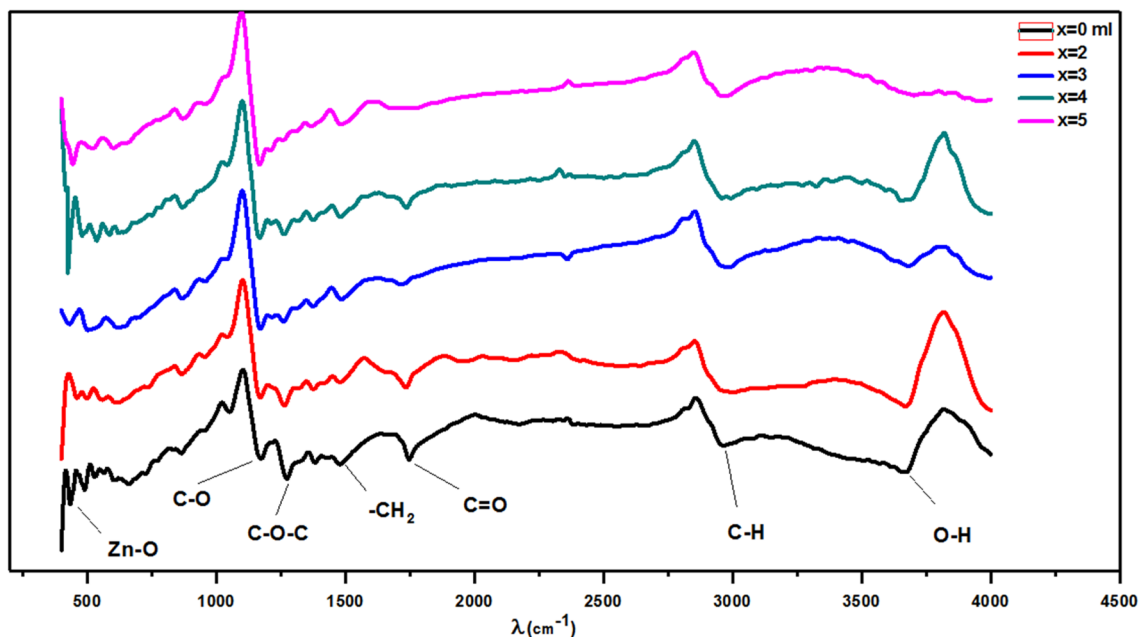


**Fig. 2** FTIR spectra of PVZO/*x*TEGDME polymer composite

**Table 1** FTIR peaks of PVZO/*x*TEGDME polymer composite

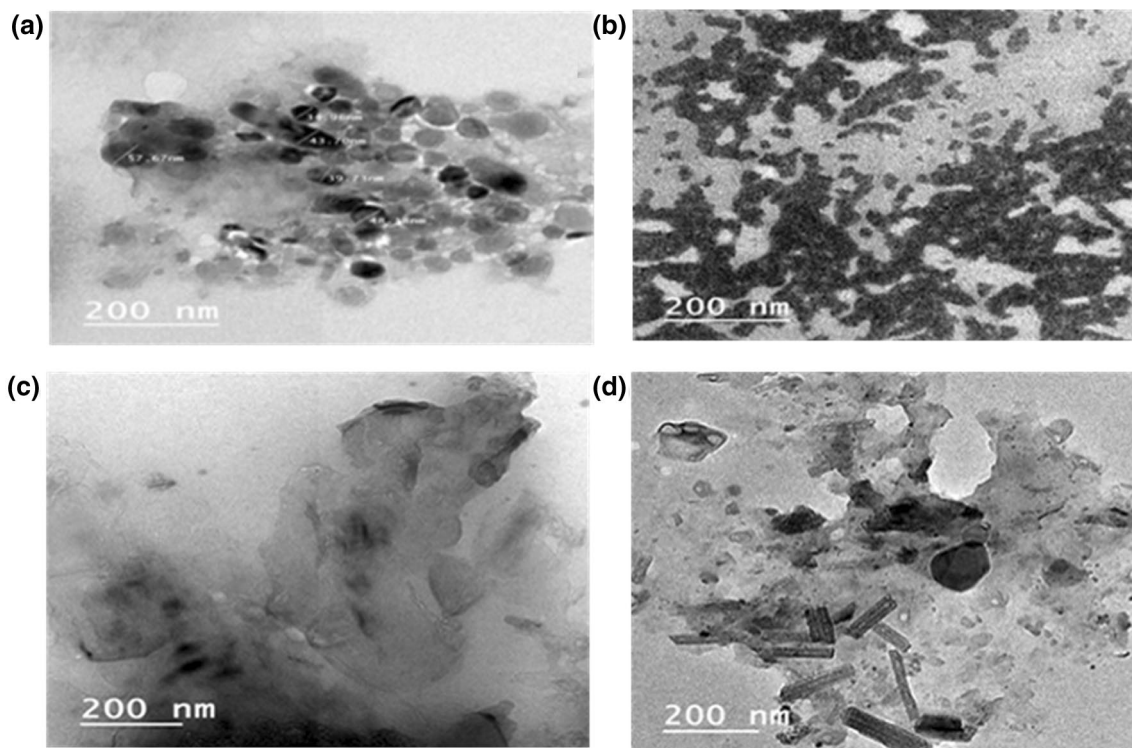
Band assignments	Wavenumber (cm <sup>-1</sup> )				
	<i>x</i> =0 ml	<i>x</i> =2 ml	<i>x</i> =3 ml	<i>x</i> =4 ml	<i>x</i> =5 ml
(O–H) stretching [23]	3623	3633	3635	3640	3647
(C–H) bending [7]	2929	2915	2919	2913	2896
C=O stretching [22]	1722	1677	1685	1677	1660
–CH <sub>2</sub> bending [24]	1421	1417	1434	1417	1427
(C–O–C)vibration [18]	1243	1230	1228	1218	1226
(C–O) stretching [18]	1151	1153	1157	1153	1155
(Zn–O) stretching [25]	432	445	430	426	437

after modifying by TEGDME. The peak at 1421 cm<sup>-1</sup> is designated as a CH<sub>2</sub> scissoring mode [24] was transferred to high order of wavenumbers after modifying by TEGDME. The peak position of Zn–O stretching vibration [25] at 432 cm<sup>-1</sup> of PVZO composite was also disturbed after modifying by TEGDME. Generally, the characteristic absorption peaks PVZO composite that transferred after modifying by TEGDME might have been related to the different chemical environment and the change in the crystallinity of the PVZO matrix as a result of physical incorporation of TEGDME [26].

The effect of TEGDME concentration on the particle size of the PVZO is shown in Fig. 3a–d. Consciously, by changing the amount of TEGDME there was an effect on particles shape compared to the pristine PVZO. Figure 3a

exhibits TEM micrograph of pristine PVZO composite. The particles of ZnO are spherical in shape, their average particle size is approximately around 50 nm and ZnO particles are immersed in PVA polymer chains and formed a homogeneous composite (PVA was shown by the white shadow on the sides of ZnO particles). Adding TEGDME changed the particle shape and crystallite distribution gradually, where the particle size of ZnO became smaller comparing with the pristine, Fig. 3b, c. The shape of the ZnO grains transformed to cylindrical nanorods when the TEGDME content was increased from 3 to 5 ml (see Fig. 3d). Cylindrical nanorods structures were found to be able to change the optical energy gap as shall be explained later.

The TGA curve of the PVZO composite with various concentrations of TEGDME is displayed in Fig. 4a. It is clear that

**Fig. 3** TEM images of PVZO/*x*TEGDME polymer composite **a** *x*=0, **b** *x*=2 ml, **c** *x*=3 ml and **d** *x*=5 ml TEGDME



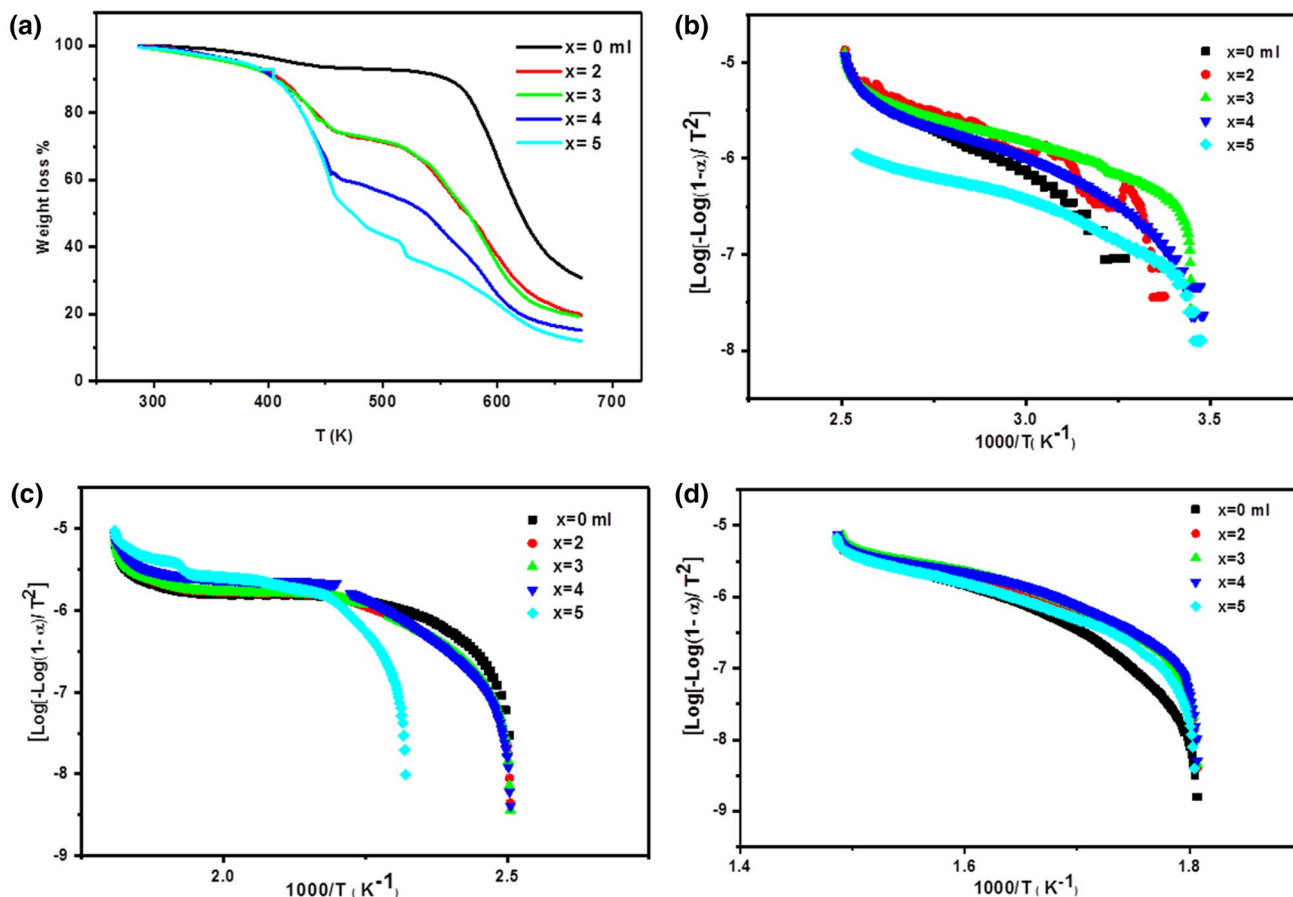


**Fig. 4** a TGA thermograms (weight loss fraction) versus temperature PVZO/*x*TEGDME polymer composite. The dependence of  $\log \left[ \frac{-\log(1-\alpha)}{T^2} \right]$  on  $1000/T$  for polymer composite at *T* range: **b** 288–398 K, **c** 398–553 K, **d** 553–673 K

the pristine PVZO composite is more stable than the modified composite with TEGDME. At 450 K, the residual mass of pristine PVZO composite is 94% from its actual value, while the residual mass is 77, 75, 65 and 58% for *x*=2, 3, 4 and 5 ml TEGDME. This asserts that TEGDME can reduce the thermal stability of pure PVZO composite. The curve showed that composites exhibit three stages of decomposition between 30 and 670 °C, due to the evaporation of physically weak H<sub>2</sub>O, the degradation of the side-chain of the PVZO composite, and the carbonation of the cleavage C–C backbone of PVA polymer film, respectively [27]. The decomposition regions are at temperature of 288–398, 398–553 and 553–673 K, respectively. The activation energy of thermal decomposition was calculated using the integral equation of Coates and Redfern [28],

$$\left[ \log \frac{-\log(1-\alpha)}{T^2} \right] = \log \left[ \frac{(1-2RT/E)AR}{\beta E} \right] - \frac{E}{2.303RT} \quad (n = 1),$$

where  $\alpha = \frac{w_i - w_t}{w_i - w_f}$ , *w<sub>i</sub>* is the initial weight, *w<sub>t</sub>* is the weight at given temperature, *w<sub>f</sub>* is the final weight of the sample,  $\beta$  is

the heating rate, *E* is the activation energy of polymer decomposition, *R* is the universal gas constant, *T* is the absolute temperature and *A* is the frequency factor. The term  $\log \left[ \frac{(1-2RT/E)AR}{\beta E} \right]$  is constant, so the relation between  $\log \left[ -\log(1-\alpha)/T^2 \right]$  and  $1000/T$  is straight line, with slope  $-E/R$ . Figure 4b-d discloses the linear fits of the Coats–Redfern equation for the three degradation steps. The values of activation energies of the thermal decomposition are listed

**Table 2** Activation energy of thermal decomposition of PVZO/*x*TEGDME polymer composite

PVZO/ <i>x</i> TEGDME <i>x</i> (ml)	Activation energy (Jmol <sup>-1</sup> )		
	Region I	Region II	Region III
0	43.97	26.38	141.97
2	37.95	36.84	103.13
3	28.35	37.19	108.32
4	39.59	42.44	103.06
5	31.10	50.27	112.36

in Table 2. From this table, it can be concluded that the addition of TEGDME could disrupt the activation energies of the thermal decomposition. This could be attributed to the low melting point of TEGDME  $\sim -30$  °C. TEGDME could reduce the viscosity of PVZO matrix; as a result, the thermal stability of the composite decreases. The small values for the thermal decomposition activation energies in the first degradation step compared with the next degradation steps confirmed the relatively lower thermal motion, higher order, and more stable structure of the materials in the first degradation step [29]. Figure 5a shows the UV–Vis absorption spectra (250–850 nm) of PVZO/*x*TEGDME colloidal in water. The spectra of pristine PVZO revealed an intense absorption band centered at approximately 290 and 380 nm arising due to the electronic transitions  $\pi \rightarrow \pi^*$  of PVA and the free exciton from the wide band gap of ZnO, respectively [25, 30–32]. It is noted from the spectra that as the content of TEGDME increased, the intensity of 290 nm absorption band decreased while the intensity of 380 nm absorption band broadened and approximately disappeared compared to pure PVZO composite. This confirms that the TEGDME perturbed the electronic structure of PVZO composite [2].

The optical energy gap of pristine PVZO composite and TEGDME modified PVZO polymer composite was determined using the frequency dependent absorption coefficient [33].

$$\alpha(\nu)h\nu = \beta(h\nu - E_g)^r$$

where  $\alpha(\nu)$  is the absorption coefficient [6] determined by  $\alpha = \left(\frac{2.303}{x}\right)A$ ,  $x$  is the thickness of the sample,  $A$  is the absorbance,  $h$  is the Planck's constant,  $\nu$  is the frequency of the incident photons,  $\beta$  is a constant which depends on the transition probability,  $E_g$  is the optical energy gap and  $r$  is an empirical index that determines the nature of the energy gap or transition [34, 35]. Theoretically,  $r$  equals 2 for indirect allowed transitions and equals 1/2 for direct allowed transitions [36, 37]. The value of index  $r$  could be determined by choosing  $r$  equal to 2 or 1/2 then plotting  $(\alpha h\nu)^r$  and photon energy ( $h\nu$ ) based on the best linear graph was obtained, the value of  $r$  was determined [34, 35]. The best linear graph was obtained by plotting  $(\alpha h\nu)^2$  as a function of photon energy  $h\nu$  (direct energy gap). The value of  $E_g$  was given by extrapolating the linear portion of the curve to the

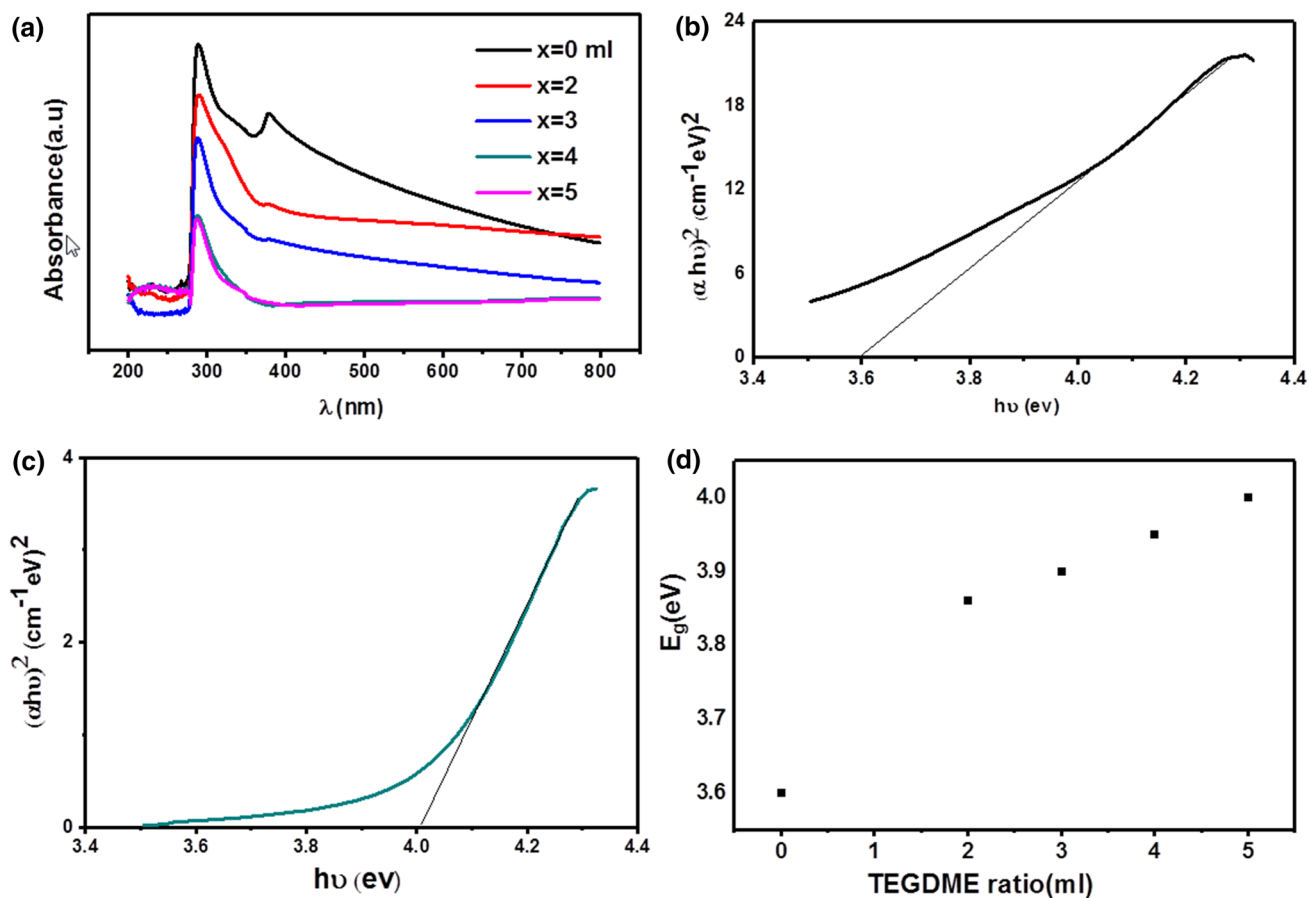


**Fig. 5** a Optical absorption spectra of PVZO/*x*TEGDME polymer composite.  $(\alpha h\nu)^2$  vs.  $h\nu$  for **b** pristine, **c**  $x=5$  ml TEGDME. **d** The optical energy gap of PVZO/*x*TEGDME composite vs. concentration of TEGDME

*hν*-axis [34] as shown in Fig. 5b, c. Figure 5d illustrates the increase in the band gap as TEGDME concentration increased, which was due to the reduction in grain size of ZnO as confirmed by TEM analysis. This could be quantum mechanically explained as follows: the particle size reached the nanoscale; the number of overlapping of orbitals or energy level decreased and the thickness of band became thinner. This caused a rise in energy band gap between the valence band and the conduction band [36]. In addition, electrons and holes in the semiconductors in nano scale are confined due to quantum confinement effect. Therefore, the energy difference between the filled states and the empty states widens the band gap of the semiconductor [37]. The ability of TEGDME to tune the optical band gap could make changes to the optical and electronic properties of semiconductors at nanoscale and made this composite potential candidate for optoelectronics devices [36, 37]. The PL measurements of PVZO/*x*TEGDME polymer composite were carried out at room temperature using  $\lambda = 350$  nm as an excitation wavelength. Figure 6a depicts the room temperature photoluminescence spectrum of pristine PVZO composite and TEGDME modified PVZO polymer composite. The pristine PVZO composite structures displayed broad band emission centered at 700 nm in the red spectral range extending to yellow and orange [38]. The intensity of the emission increased with increasing the ratio of TEGDME. This could be attributed to the decrease in estimated crystallite size at

higher molar concentration of TEGDME and the increase in transparency due to full dissolving of ZnO. Furthermore, the increase in the band broadening could be associated with the internal defects (oxygen vacancies or zinc interstitials) in PVZO composite [8, 39] due to the introduction of TEGDME as shown in the proposed schematic diagram of electronic transitions, Fig. 6b [40–42]. The variation of photoemission intensity of PVZO composite with the TEGDME concentration is shown in Fig. 6c. It is clearly seen that the PL intensity increases polynomial with the increasing of TEGDME ratio where the optimum luminescence intensity is at a concentration 5 ml TEGDME. TEGDME concentration was linked with PL intensity via fitting the second order equation:  $y = 34.89x^2 - 45.095x + 165.34$ . It was observed that, as the concentration  $\sim 0$ , the PL intensity  $\sim 165.34$  which coincided with the experimental data. In general, we could determine the PL intensity at any concentration of TEGDME. The full width at half maximum FWHM of PL peak had been estimated from Fig. 6a and was presented in Fig. 6d as a function of TEGDME content. It was observed that the FWHM increased polynomial with increasing TEGDME content according to the second order equation  $y = 0.0558x^2 + 0.9889x + 19.817$ . This confirmed that modifying PVZO composite with TEGDME supported the formation of new radiative recombination centers. Figure 7a exhibits the variation of the dielectric constant  $\epsilon'$  with applied frequency at room temperature for pristine PVZO

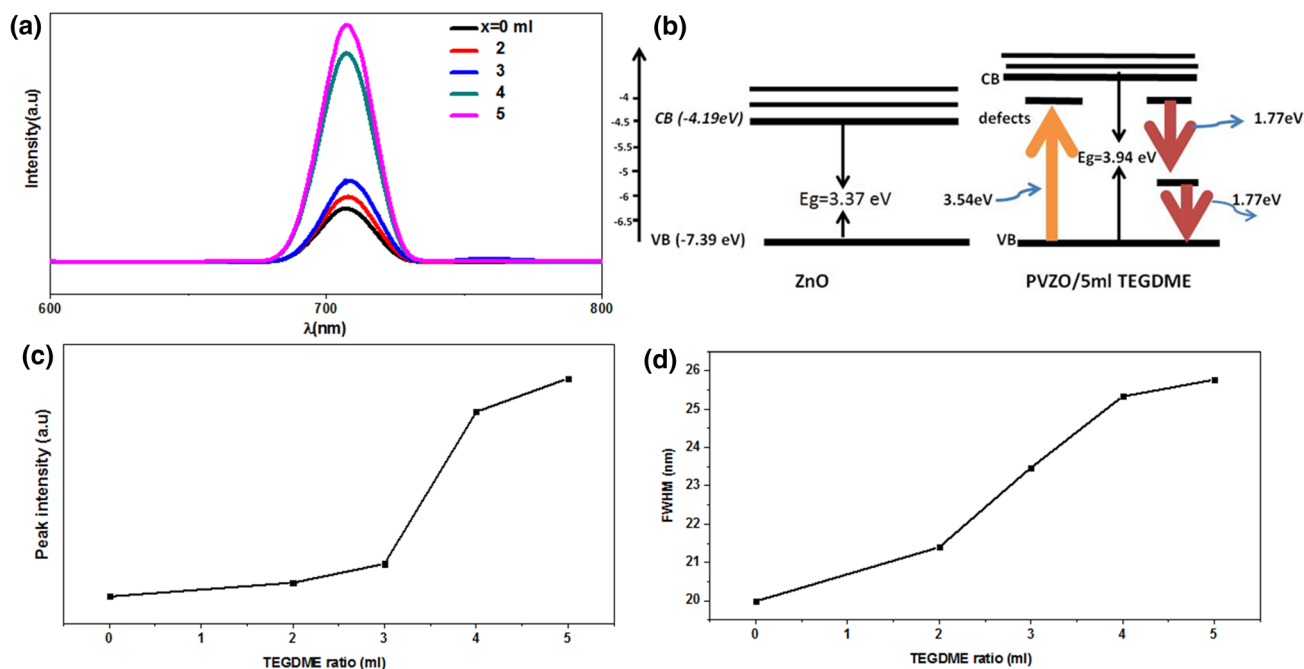


**Fig. 6** **a** Photoluminescence (PL) spectra of PVZO/*x*TEGDME polymer composite, **b** the schematic diagram of electronic transition of PVZO/5 ml TEGDME. **c** The dependence of photoemission intensity

on the concentration of TEGDME. **d** The dependence of photoluminescence FWHM on the concentration of TEGDME

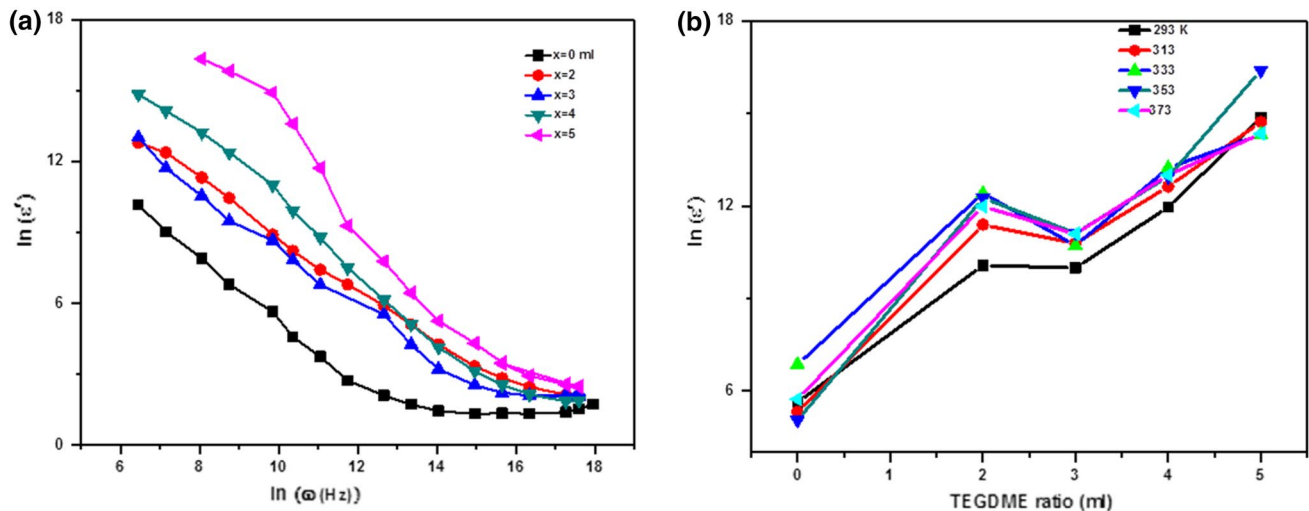


**Fig. 7** Plot of **a**  $\ln(\epsilon')$  vs.  $\ln \omega$  at 30 °C, **b**  $\ln(\epsilon')$  vs. concentration of PVZO/ $x$ TEGDME polymer composite

and TEGDME modified PVZO polymer composite. The dielectric constant decreases with an increase in the frequency. This behavior is due to the fact that, moving to higher frequencies, the bigger dipolar groups do not have sufficient time to align before the field changes its directions, so the contributions of these dipolar groups to the relative permittivity goes on in a continuously decreasing manner [43]. The variation of dielectric constant  $\epsilon'$  of PVZO composite with the TEGDME concentration is shown Fig. 7b. It is clearly seen that, the dielectric constant  $\epsilon'$  increases with the increase of TEGDME ratio. TEGDME was able to reduce the viscosity of pristine PVZO composite, and released free charge carriers from wurtzite structure. This might have been the cause behind the increase of the dielectric constant  $\epsilon'$  [43]. The enhancement of the dielectric constant significantly influenced the exciton binding energy; the resulting charge separation and recombination result in improvement photocurrent, short-circuit current densities ( $J_{sc}$ ) and power conversion efficiencies (PCEs) [11, 12].

As a result, this composite is a potential candidate for optoelectronics devices. Figure 8a shows the variation of the ac conductivity  $\sigma_{ac}(\omega)$  with applied frequency at room temperature for PVZO/ $x$ TEGDME polymer composite. This frequency response could be divided into two regions: (1) low frequency plateau, (2) high frequency dispersive region. The high frequency dispersion was attributed to increased rate of hopping through grain boundaries by the charge carriers whereas the low frequency plateau was due to diffusion of charge. This behavior follows a universal power law [44].

$$\sigma_{ac}(\omega) = \sigma_{dc} + A\omega^S$$

where  $\sigma_{dc}$  is the dc conductivity (the extrapolation of the plateau region to zero frequency),  $\omega$  is the angular frequency,  $A$  is a temperature and angular frequency dependent

constant and  $S$  is an exponent generally equal or less than unity and usually used to characterize the ac conduction in various semiconducting materials. The power exponent was acquired from the slope of  $\ln \sigma_{ac}$  vs.  $\ln \omega$  plotted at different temperatures [39]. The value of  $0.5 > S > 1$  might have been due to the collective motion of polarons in the short-range order which is the most suitable mechanism to explain the ac conduction behavior in these polymer electrolyte [44]. Figure 8b indicates that the variation of the temperature has no significant effect on  $\sigma_{ac}$ . The variation of dc conductivity (calculated from the linear fit of ac conductivity spectra at  $\omega=0$ ) of PVZO composite with the TEGDME concentration is shown in Fig. 8c. Conspicuously, dc conductivity increases with the increase of TEGDME ratio. This behavior could be analyzed using conductivity-mobility  $\mu$  relation [45]:

$$\mu = \frac{De}{k_B T}$$

$$\sigma = ne\mu,$$

where  $D$  is the diffusion coefficient,  $e$  is the elementary charge,  $k_B$  is the Boltzman's constant,  $\sigma$  is the room temperature conductivity and  $T$  is the temperature. As mentioned before, TEGDME could drop the viscosity of PVZO composite and enhance the diffusion coefficient. The increase of the diffusion coefficient means increase of charge carrier mobility and hence the conductivity. It is noted that, the deviation from the dc conductivity plateau to the high frequency dispersive region is at the hopping frequency ( $\omega_p$ ). The obtained values of  $\omega_p$  shift to higher frequencies with increasing TEGDME ratio obeying the following empirical relation  $y = -0.0383x^2 + 0.6505x - 14.568$ . The variation of  $\omega_p$  with the TEGDME concentration is shown in Fig. 8d.



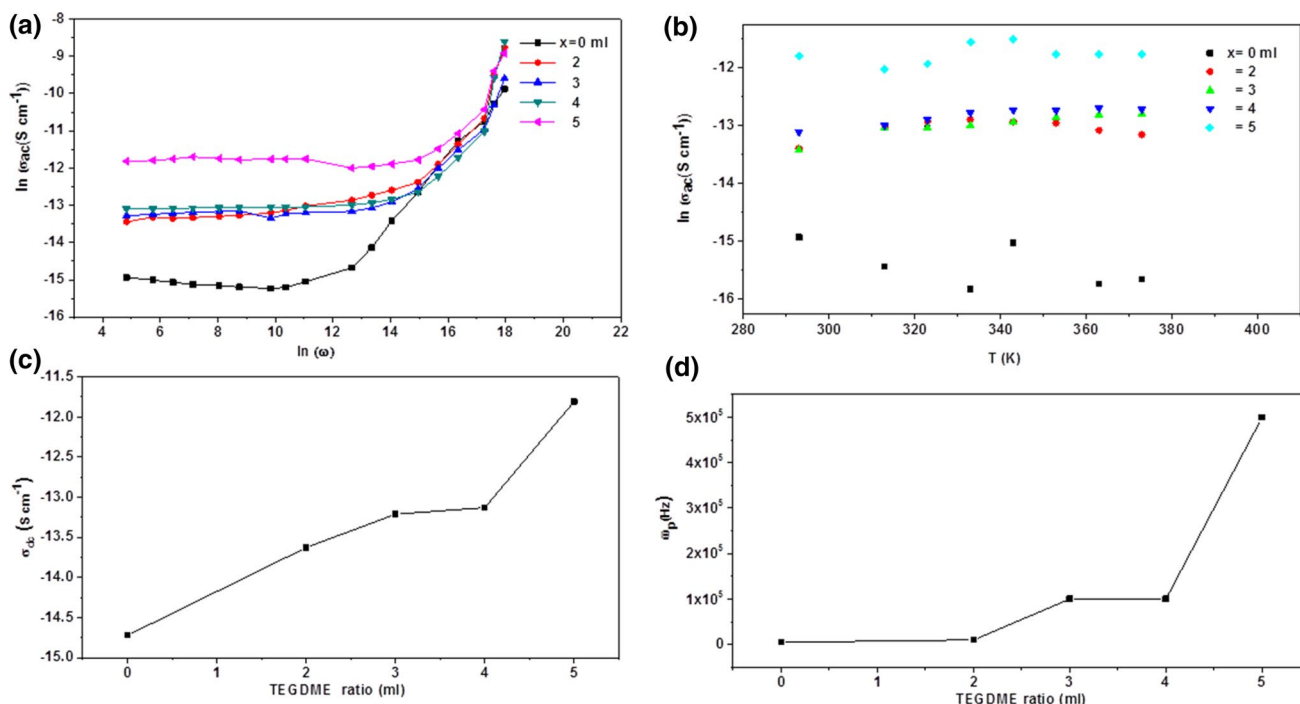


**Fig. 8** Plot of **a**  $\ln(\sigma_{ac})$  vs.  $\ln \omega$  at 30 °C, **b**  $\ln(\sigma_{ac})$  vs. temperature at 1 kHz of PVZO/ $x$ TEGDME polymer composite. **c** The dependence of the dc conductivity  $\sigma_{dc}$  on the concentration of TEGDME. **d** The dependence of the hopping frequency ( $\omega_p$ ) on the concentration of TEGDME

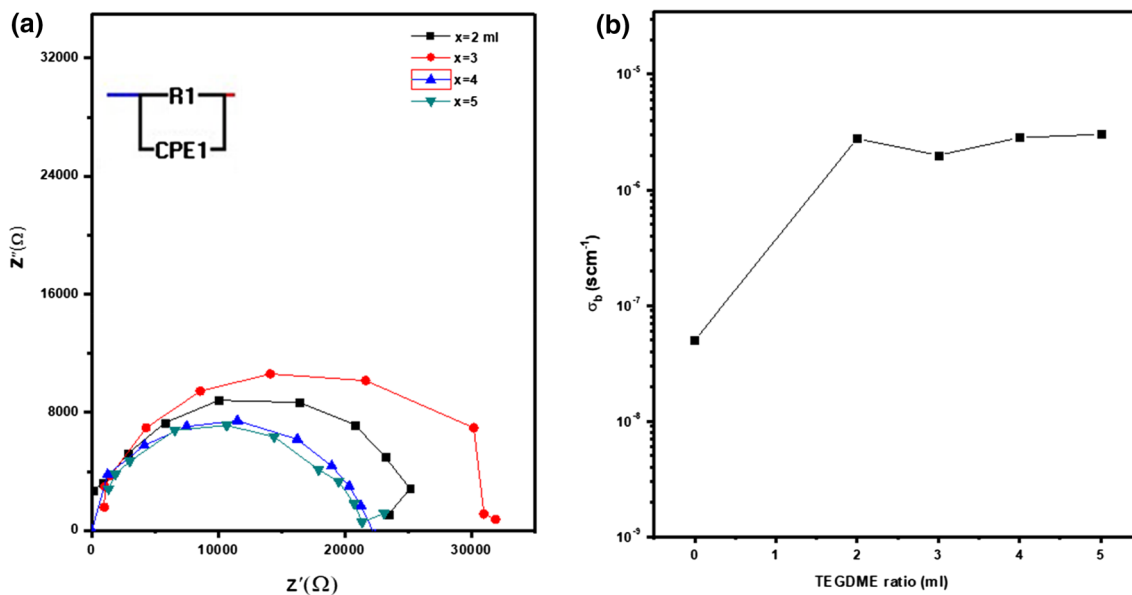


**Fig. 9** **a** Cole–Cole plots of PVZO/ $x$ TEGDME polymer composite at room temperature; the inset is the equivalent circuit, **b** the dependence of bulk conductivity  $\sigma_b$  on the concentration of TEGDME

It is obvious that,  $\omega_p$  increases with the increase of TEGDME ratio. This could be attributed to the fact that the introduction of TEGDME was able to increase the diffusion coefficient of charge carrier which shifted the threshold frequency to higher values. Figure 9a represents the

Cole–Cole plots for PVZO composite at different TEGDME concentrations. Typical sole semicircle could be traced, the diameter of the semicircle decreases with increasing TEGDME concentrations. The formation of semi arc indicated the parallel geometrical capacitance to the bulk resistance

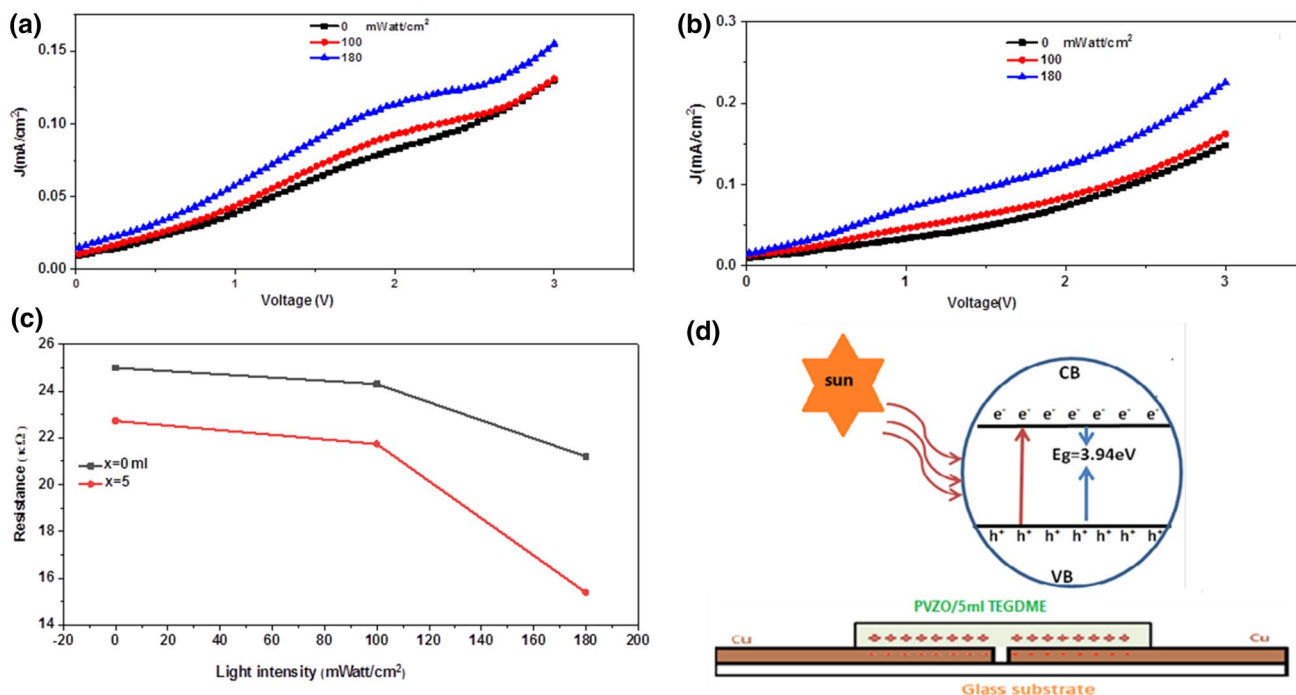


**Fig. 10**  $J$ - $V$  curves of **a** pristine, **b** 5 ml TEGDME modified PVZO polymer composite, under various sun light intensity, **c** resistance dependence of PVZO/ $x$ TEGDME polymer composite on sun light intensity. **d** The schematic diagram of the fabricated cell and charges generation

as shown in the inset of Fig. 9a [46]. The bulk conductivity  $\sigma_b$  for the PVZO/TEGDME polymer composites was calculated using the Cole–Cole plots by the given relation  $\sigma_b = \frac{L}{R_b A}$  [44], where  $L$  is the film thickness and  $A$  is its effective area. It is clear from Fig. 9b that, the bulk conductivity  $\sigma_b$  increases as TEGDME ratio increases. The light sensitivity for the pristine PVZO and PVZO/5 ml TEGDME gel was calculated by measuring the  $J$ - $V$  characteristics in dark and illumination as shown in Fig. 10a, b. Obviously, this composite is very sensitive to light, where the current density increases with increasing the light intensity. By fitting the data of  $J$ - $V$  curves, the slope could be determined and the resistance of the composite was calculated. The relation between the resistances of the composite with the light intensity is shown in Fig. 10c. The resistance of the composite decreases with increasing the light intensity and the PVZO/5 ml TEGDME has lower resistance compared to the pristine PVZO composite. This is due to the introduction of TEGDME is able to increase the dielectric constant which enhance the charge carriers generation, photocurrent and current density. In addition, TEGDME increases the transparency of the composite which improves the probability of photons–electrons interaction in the valence band. Schematic diagram of the fabricated cell is shown in Fig. 10d.

## 4 Conclusions

This research presented a convenient and effective technique to improve the performance of PVZO composite via modifying it by TEGDME with the intention of modulating the dielectric constant. Increasing the content of TEGDME units gradually reduced the ZnO crystallite size, improved the charge generation largely and improved the dielectric constant. XRD and TEM results ascertained that, TEGDME succeeded in dissolving ZnO particles to nanoscale and dispersing it uniformly in the host matrix. As a result, the optical band gap modulated from 3.6 to 4 eV due to the reduction of the particle size. TEGDME enhanced the intensity and broadening of visible photoemission around 700 nm via formation of new radiative recombination centers. The tunable dielectric properties and high robustness of (PVA/ZnO)/TEGDME composites make them promising candidates for light emitting devices with low power consumption. This work opens a new avenue for molecular design of optical polymer composites for high-performance.

**Acknowledgements** Funding was provided by Benha University and National Institute of standards.

## References

- X.M. Zhang, M.Y. Lu, Y. Zhang, L.J. Chen, Z.L. Wang, Fabrication of a high-brightness blue-light-emitting diode using a ZnO-nanowire array grown on p-GaN thin film. *Adv. Mater.* **21**, 2767–2770 (2009)
- O. Elkalashy, E. Sheha, R. Khalil, E. Elmoghazy, Evaluate the effect of super P carbon black on tuning the optical and photometric properties of PVA–ZnO composite. *J. Nanoelectron. Optoelectron.* **13**(3), 349–356 (2018)
- J. Lee, D. Kim, K. Kim, T. Seong, Reducing forward voltage and enhancing output performance of diodes using metal dot-embedded transparent p-type finger. *Phys. Status Solidi (a)* **214**(8), 1600792 (2017)
- N.X. Sang, T. Chuan, T. Jie, E.A. Fitzgerald, C.S. Jin, Fabrication of p-type Zn O nanorods/n-G a N film heterojunction ultraviolet light-emitting diodes by aqueous solution method. *Phys. Status Solidi* **1623**, 1618–1623 (2013)
- S. Kakarndee, S. Nanan, SDS capped and PVA capped ZnO nanostructures with high photocatalytic performance toward photodegradation of reactive red (RR141) azo dye. *J. Environ. Chem. Eng.* **6**, 74–94 (2018)
- M.H. Habibi, B. Karimi, M. Zendehtdel, M. Habibi, Fabrication, characterization of two nano-composite CuO–ZnO working electrodes for dye-sensitized solar cell. *Spectrochim. Acta Part A Mol. Biomol. Spectrosc.* **116**, 374–380 (2013)
- E. Ghafari, Y. Feng, Y. Liu, I. Ferguson, N. Lu, Investigating process-structure relations of ZnO nanofiber via electrospinning method. *Compos. Part B Eng.* **116**, 40–45 (2017)
- H.N. Chandrakala, B. Ramaraj, J.H. Lee, Siddaramaiah, polyvinyl alcohol/carbon coated zinc oxide nanocomposites: electrical, optical, structural and morphological characteristics. *J. Alloys Compd.* **580**, 392–400 (2013)
- Y.S. Tamgadge, A.L. Sunatkari, S.S. Talwatkar, V.G. Paturkar, G.G. Muley, Passive optical limiting studies of nanostructured Cu doped ZnO–PVA composite thin films. *Opt. Mater. (Amst)* **51**, 175–184 (2016)
- M.Y. Soomro, S. Hussain, N. Bano, I. Hussain, O. Nur, M. Willander, Hybrid organic zinc oxide white-light-emitting diodes on disposable paper substrate. *Phys. Status Solidi* **1605**, 1600–1605 (2013)
- X. Xu, Z. Li, J. Wang, B. Lin, W. Ma, Y. Xia, M.R. Andersson, R.A.J. Janssen, E. Wang, High-performance all-polymer solar cells based on fluorinated naphthalene diimide acceptor polymers with fine-tuned crystallinity and enhanced dielectric constants. *Nano Energy* **45**, 368–379 (2018)
- B. Jang, C. Lee, Y.W. Lee, D. Kim, M.A. Uddin, F.S. Kim, B.J. Kim, H.Y. Woo, A high dielectric N-type small molecular acceptor containing oligoethyleneglycol side-chains for organic solar cells. *Chin. J. Chem.* **36**, 199–205 (2018)
- A.N. Aleshin, I.P. Shcherbakov, V.N. Petrov, A.N. Titkov, Solution-processed polyfluorene–ZnO nanoparticles ambipolar light-emitting field-effect transistor. *Org. Electron.* **12**, 1285–1292 (2011)
- M.B. Upama, N.K. Elumalai, M.A. Mahmud, M. Wright, D. Wang, C. Xu, A. Uddin, Effect of annealing dependent blend morphology and dielectric properties on the performance and stability of non-fullerene organic solar cells. *Sol. Energy Mater. Sol. Cells* **176**, 109–118 (2018)
- A. Genssle, K. Stephan, Analysis of the process characteristics of an absorption heat transformer with compact heat exchangers and the mixture TFE–E181. *Int. J. Therm. Sci.* **39**, 30–38 (2000)
- H.S. Ryu, H.J. Ahn, K.W. Kim, J.H. Ahn, K.K. Cho, T.H. Nam, J.U. Kim, G.B. Cho, Discharge behavior of lithium/sulfur cell with TEGDME based electrolyte at low temperature. *J. Power Sources* **163**, 201–206 (2006)
- M. Kartal, A. Alp, H. Akbulut, Electrical conductivity, viscosity and thermal properties of tegdme-based composite electrolytes for lithium-air batteries. *Acta Phys. Pol. A* **129**, 816–818 (2016)
- X. Gong, C.Y. Tang, L. Pan, Z. Hao, C.P. Tsui, Characterization of poly(vinyl alcohol) (PVA)/ZnO nanocomposites prepared by a one-pot method. *Compos. Part B Eng.* **60**, 144–149 (2014)
- B. Karthikeyan, T. Pandiyarajan, R.V. Mangalaraja, Enhanced blue light emission in transparent ZnO:PVA nanocomposite free standing polymer films. *Spectrochim. Acta Part A Mol. Biomol. Spectrosc.* **152**, 485–490 (2016)
- L.C. Liao, Y. Lin, Effects of electric fields on the conduction of polyvinyl alcohol (PVA)/ZnO films by photoluminescence analysis. *J. Lumin.* **181**, 217–222 (2017)
- N. Kwietniewski, M. Maslyk, A. Werbowy, A. Taube, S. Gieratowska, Ł. Wachnicki, M. Sochacki, Electrical characterization of ZnO/4H–SiC n-p heterojunction diode. *Phys. Status Solidi Appl. Mater. Sci.* **213**, 1120–1124 (2016)
- M.H. Habibi, M.H. Rahmati, Fabrication and characterization of ZnO@CdS core-shell nanostructure using acetate precursors: XRD, FESEM, DRS, FTIR studies and effects of cadmium ion concentration on band gap. *Spectrochim. Acta Part A Mol. Biomol. Spectrosc.* **133**, 13–18 (2014)
- D. Kumar, N. Vijayan, S. Banerjee, Synthesis, characterization, and studies of PVA/co-doped ZnO nanocomposite films. *Int. J. Green Nanotechnol.* **4**(3), 408–416 (2012)
- X. Gong, C. Yin, L. Pan, Z. Hao, C. Pong, Composites: part B characterization of poly (vinyl alcohol) (PVA)/ZnO nanocomposites prepared by a one-pot method. *Compos. Part B* **60**, 144–149 (2014)
- K.S. Hemalatha, K. Rukmani, N. Suriyamurthy, B.M. Nagabhushana, Synthesis, characterization and optical properties of hybrid PVA–ZnO nanocomposite: a composition dependent study. *Mater. Res. Bull.* **51**, 438–446 (2014)
- A. Akhavan, F. Khoylou, E. Ataievarjovi, Preparation and characterization of gamma irradiated Starch/PVA/ZnO nanocomposite films. *Radiat. Phys. Chem.* **138**, 49–53 (2017)
- J.J. Mathen, J. Madhavan, A. Thomas, A.J. Edakkara, J. Sebastian, G.P. Joseph, Transparent ZnO–PVA binary composite for UV-A photo detector: optical, electrical and thermal properties followed by laser induced fluorescence. *J. Mater. Sci. Mater. Electron.* **28**, 7190–7203 (2017)
- L.A.A Pérez-Maqueda, P.E.E. Sánchez-Jiménez, J.M.M. Criado, Evaluation of the integral methods for the kinetic study of thermally stimulated processes in polymer science. *Polymer* **46**, 2950–2954 (2005)
- M.M. Abdel-Kader, M.A.F. Basha, G.H. Ramzy, A.I. Aboud, Thermal and ac electrical properties of N-methylanthranilic acid below room temperature. *J. Phys. Chem. Solids* **117**, 13–20 (2018)
- G. Attia, M.F.H.A. El-kader, Structural, optical and thermal characterization of PVA/2HEC polyblend films. *Int. J. Electrochem. Sci.* **8**, 5672–5687 (2013)
- L.F. Koao, B.F. Dejene, F.G. Hone, H.C. Swart, S.V. Motloung, T.E. Motaung, V.B. Pawade, Effects of octadecylamine molar concentration on the structure, morphology and optical properties of ZnO nanostructure prepared by homogeneous precipitation method. *J. Lumin.* **200**, 206–215 (2018)
- N. Bouropoulos, G.C. Psarras, N. Moustakas, A. Chrissanthopoulos, S. Baskoutas, Optical and dielectric properties of ZnO–PVA nanocomposites. *Phys. Status Solidi Appl. Mater. Sci.* **205**, 2033–2037 (2008)
- M. Saleem, A. Manzoor, M. Zaffar, S.Z. Hussain, M.S. Anwar, Tailoring of ZnO with selected group-II elements for LED materials. *Appl. Phys. A Mater. Sci. Process.* **122**, 1–8 (2016)

34. H.M. Shanshool, M. Yahaya, W.M.M. Yunus, I.Y. Abdullah, Investigation of energy band gap in polymer/ZnO nanocomposites. *J. Mater. Sci. Mater. Electron.* **27**, 9804–9811 (2016)
35. K. Al-ammam, A. Hashim, M. Husaien, Synthesis and study of optical properties of (PMMA-CrCl<sub>2</sub>) composites. *Chem. Mater. Eng.* **1**, 85–87 (2013)
36. M. Singh, M. Goyal, K. Devlal, Size and shape effects on the band gap of semiconductor compound nanomaterials. *J. Taibah Univ. Sci.* **12**(4), 470–475 (2018)
37. M.B. Sahana, C. Sudakar, A. Dixit, J.S. Thakur, R. Naik, V.M. Naik, Quantum confinement effects and band gap engineering of SnO<sub>2</sub> nanocrystals in a MgO matrix. *Acta Mater* **60**, 1072–1078 (2012)
38. Kishwar, K.u. Hasan, G. Tzamalīs, O. Nur, M. Willander, H. Kwack, D.L.S. Dang, Electro-optical and cathodoluminescence properties of low temperature grown ZnO nanorods/p-GaN white light emitting diodes. *Phys. Status Solidi (a)* **207**(1), 67–72 (2010)
39. A.M. Abdelghany, H.M. Zeyada, H.A. ElBatal, R.E. Fetouh, AC conductivity and dielectric behavior of silicophosphate glass doped by Nd<sub>2</sub>O<sub>3</sub>. *Silicon* **9**, 347–354 (2017)
40. L.-J. Tzeng, C.-L. Cheng, Y.-F. Chen, Enhancement of band-edge emission induced by defect transition in the composite of ZnO nanorods and CdSe/ZnS quantum dots. *Opt. Lett.* **33**, 569–571 (2008)
41. S.S. Wilson, J.P. Bosco, Y. Tolstova, D.O. Scanlon, G.W. Watson, H.A. Atwater, Interface stoichiometry control to improve device voltage and modify band alignment in ZnO/Cu<sub>2</sub>O heterojunction solar cells. *Energy Environ. Sci.* **7**, 3606–3610 (2014)
42. J.C. Medina, N.S. Portillo-Vélez, M. Bizarro, A. Hernández-Gordillo, S.E. Rodil, Synergistic effect of supported ZnO/Bi<sub>2</sub>O<sub>3</sub> heterojunctions for photocatalysis under visible light. *Dyes Pigments* **153**, 106–116 (2018)
43. H.M. El-Mallah, AC electrical conductivity and dielectric properties of perovskite (Pb, Ca) TiO<sub>3</sub> ceramic. *Acta Phys. Pol. A* **122**, 174–179 (2012)
44. E. Sheha, H. Khoder, T.S. Shanap, M.G. El-Shaarawy, M.K. El Mansy, Structure, dielectric and optical properties of p-type (PVA/CuI) nanocomposite polymer electrolyte for photovoltaic cells. *Optik (Stuttg)* **123**, 1161–1166 (2012)
45. H.K. Koduru, L. Marino, F. Scarpelli, A.G. Petrov, Y.G. Marinov, G.B. Hadjichristov, M.T. Iliev, N. Scaramuzza, Structural and dielectric properties of NaIO<sub>4</sub>—complexed PEO/PVP blended solid polymer electrolytes. *Curr. Appl. Phys.* **17**, 1518–1531 (2017)
46. A.S. Roy, S. Gupta, S. Sindhu, A. Parveen, P.C. Ramamurthy, Composites: part B dielectric properties of novel PVA/ZnO hybrid nanocomposite films. *Compos. Part B* **47**, 314–319 (2013)